Citation for published version:
Bull, S, Chiereghin, N & Cleaver, D 2022, 'Compounding Transient Airfoil Motions and the Effectiveness of Linear Superposition', *AIAA Journal*. https://doi.org/10.2514/1.J061640

DOI:
10.2514/1.J061640

Publication date:
2022

Document Version
Peer reviewed version

Link to publication

Publisher Rights
CC BY

© 2022 American Institute of Aeronautics and Astronautics

University of Bath

Alternative formats
If you require this document in an alternative format, please contact:
openaccess@bath.ac.uk

General rights
Copyright and moral rights for the publications made accessible in the public portal are retained by the authors and/or other copyright owners and it is a condition of accessing publications that users recognise and abide by the legal requirements associated with these rights.

Take down policy
If you believe that this document breaches copyright please contact us providing details, and we will remove access to the work immediately and investigate your claim.

Download date: 23. Sep. 2022

Compounding Transient Airfoil Motions and the Effectiveness of Linear Superposition

Sam Bull*, Nicola Chiereghin†, and David J. Cleaver‡

The University of Bath, Bath, Somerset, BA2 7AY, United Kingdom

Abstract

This paper investigates, for the first time, the effects of compounding transient airfoil motions and the predictive capability of the linear superposition principle in vortex dominated flows. Significant increases in peak lift and nose-down pitching moment were observed during the second of two transient plunging motions at a post-stall angle of attack. The load response of the second motion was estimated through linear superposition of the first motion response with a surprising level of accuracy. Flow field measurements revealed this performance to coincide with a constructive merging of Leading-Edge Vortices (LEVs). LEV merging showed sensitivity to motion timing. Breakdown of the linear superposition prediction coincided with LEV detachment and Trailing-Edge Vortex (TEV) formation, which disrupted constructive LEV merging. The amplitude of the second motion showed no discernible effect on LEV merging and subsequently the accuracy of the linear superposition prediction. An extension to periodic motion was investigated, where linear superposition of a single sinusoidal cycle was compared with the true periodic response. This was found to capture the mean lift increase for low to moderate reduced frequencies. Lift amplitude however was captured with reasonable accuracy across the range of reduced frequencies and amplitudes tested.

Nomenclature

A/c	=	normalized plunging amplitude
α_0	=	geometric angle of attack, ^{o}
α_{pl}	=	plunging induced angle of attack, ^{o}
$\alpha_{pl,peak}$	=	maximum plunging induced angle of attack, ^{o}
c	=	chord length, m
C_l	=	lift coefficient

* Lecturer, Department of Mechanical Engineering, corresponding author, s.c.bull@bath.ac.uk
† Research Associate, Department of Mechanical Engineering
‡ Senior Lecturer, Department of Mechanical Engineering

C_m = pitching moment coefficient

ΔC_l = change in lift coefficient relative to static conditions

ΔC_m = change in pitching moment coefficient relative to static conditions

$\Delta\tau$ = convective time delay between transient motions

h/c = *normalized plunge position*

k = reduced frequency, $\pi fc/U_\infty$

t = time, s

τ = convective time, tU_∞/c

U_∞ = freestream velocity, m/s

ω_z = spanwise vorticity, s^{-1}

Subscripts

A = motion A

B = motion B

1,2,3 = vortex number in shedding cycle

I. Introduction

Leading-Edge Vortices (LEVs) have been a subject of interest across many engineering fields due to their link with high lift production. They can occur during extreme, unsteady aerodynamic events where flow at the wing's leading-edge will separate and roll-up into a single, coherent vortical structure, the LEV. The behavior of the LEV, and its subsequent effect on the aerodynamic loading, is highly non-linear and notoriously difficult to predict. Studies of periodic unsteadiness, such as flapping flight and helicopter rotor blades, have provided valuable insight into key mechanisms and their scaling with input parameters, but critical LEV physics are too often obscured by the imposed wing motion [1]. To remedy this, researchers have sought to distill the problem into canonical transient disturbances to better isolate and understand the salient aerodynamic responses. This has resulted in advancements in understanding of LEV behavior during transient pitch [2-4], plunge [4-6], surge [2, 7, 8] and discrete gust [9-12] events. These canonical cases serve as building blocks of understanding for more complex and realistic scenarios, where canonical disturbances can act in combination and quick succession. Such scenarios however are likely to produce complex flow fields with

strong interaction between vortical structures, leading to greater uncertainty in our understanding and predictive capabilities. As outlined by Eldredge and Jones [1], canonical transient motion combinations need to be examined to determine the bulk flow field response, where there is comparatively little understanding of the LEV behavior.

Through the introduction of additional and potentially different transient events the parameter space increases considerably, producing an infeasible number of test cases [7]. A somewhat optimistic solution for parameter space reduction would be through the application of the linear superposition principle; that is, can the response to multiple transient events be estimated through the sum of their individual responses? The word *estimated* is appropriate here, because is obvious that with such a high degree of non-linearity, linear superposition will always be an approximation. This is put rather succinctly by Eldredge and Jones:

> *"…it is abundantly clear that no such principle can exist in these large-amplitude motions with highly nonlinear fluid dynamics."*
>
> — Eldredge and Jones [1]

Nevertheless, the use of linear superposition in such flows is not a new concept [13-15]. Mulleners *et al.* [7] found the lift response of a transient surging flat plate to be largely independent of the initial flow conditions, i.e. vorticity distribution, leading them to postulate the following:

> *"If the response to a single gust is mostly independent of the initial state of the flow, the response to a succession of gusts… should be the result of the linear superposition of the individual responses, even though each encounter may be characterized by nonlinear effects."*
>
> — Mulleners *et al.* [7]

These two quotes are in direct contrast, yet both contain their own merit and warrant investigation. This paper therefore explores the aerodynamic response of an airfoil to compounding transient plunging motions and where, if at all, the principle of linear superposition can be applied.

II. Methods and Techniques

A. Experimental Setup

This study considers a NACA 0012 airfoil undergoing plunging motions at a Reynolds number of 20,000. Experiments were performed in The University of Bath's closed-loop water tunnel facility, which can provide up to 0.5 m/s at a free-stream turbulence intensity less than 0.5% [16] to a working test section of 381 x 508 x 1530 mm^3. The wing was manufactured with a chord length, c, of 62.7 mm and a span of 313.5 mm using selective laser sintering of PA 2200 polyamide, sanded smooth and painted matt black to reduce reflectivity. Spanwise rigidity of the wing was increased through a 25 mm by 5 mm carbon fibre bar inserted through the wing at a chordwise position $x/c = 0.25c$. Plunging motion and loads measurements are provided by the experimental rig shown in Figure 1. The wing is positioned vertically in the test section and capped at both ends by stationary splitter plates to establish quasi-2D conditions, see Figure 1a. A third moving splitter plate is placed at the top of wing to mask the slot in the upper splitter plate (Figure 1b) and mitigate any free-surface effects. This extends $0.15c$ upstream and downstream of the leading and trailing-edges respectively, and $\pm 0.08c$ in the cross-stream direction. Gaps between the moving and stationary parts were no greater than $0.02c$.

The wing attaches to the moving carriage above via a rotation stage, which can set the angle of attack (α_0) within ±0.2º, that is mounted to the underside of a torque sensor (Figure 1a). The moving carriage is fixed to a pair of shafts that each pass through a set of air bushings to constrain motion to the plunging axis. Closed-loop plunging motion is provided by a Zaber LSQ150B-T3 translation stage powered by a stepper motor with an X-MCB1 controller.

B. Load Measurements

Lift measurements are provided by a Futek S-beam tension/compression load cell (FSH00103) which runs parallel to the plunging axis and acts as a link between the translation stage and moving carriage. This configuration is enabled through the air bearing assembly, which absorbs the large bending and torque loads from the moving assembly and allows a relatively sensitive load cell to be used for dynamic measurements. Pitching moment measurements are provided by a Futek reaction torque sensor (FSH03990) that is aligned with the quarter-chord axis of the wing. Finally, a StrainSense 4807A accelerometer is mounted to the moving carriage to provide acceleration measurements of plunging motion. The acceleration signal is used to subtract the

inertial load of the moving assembly from the total loads captured by the force/torque transducers, isolating the aerodynamic components. Inertial loads are calculated through the product of the instantaneous acceleration signal and the moving mass associated with each sensor. With the aerodynamic component isolated, an ensemble-average is taken over 30 repeats of each case to remove the out-of-phase noise components. Note that this will also suppress any unsteady loads that are not phase-locked to the airfoil motion. The signals are

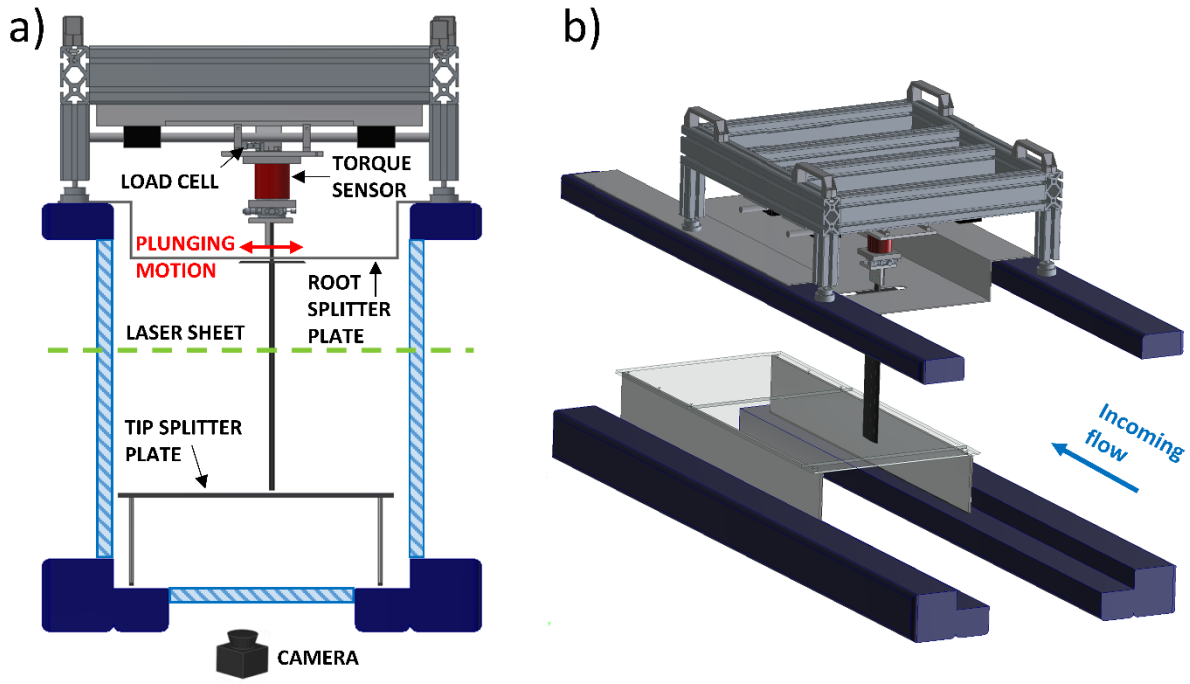

Figure 1: Experimental test rig a) front view, b) isometric view

then split at the point of initial motion acceleration and passed through a set of 3rd order Butterworth band-stop filters to remove the dominant structural frequencies of the wing (8.1 Hz) and moving carriage assembly (32 Hz, 40 Hz). The independently filtered signals are re-appended, and any discontinuities are removed by a 50 Hz moving average filter. This method avoids any unphysical smoothing of the loads at the point of initial motion acceleration and preserves the sharp change observed in the unfiltered signals. Uncertainties in the lift and pitching moment coefficients change between static and dynamic conditions (during wing motion). The uncertainty in C_l is estimated to be ±0.04 in static conditions, and ±0.15 in dynamic conditions. For the pitching moment, the uncertainty in C_m is estimated to be ±0.005

in static conditions and ±0.015 in dynamic conditions [17]. Measurements were obtained at a rate of 2000 samples per motion period.

C. Particle Image Velocimetry Measurements

Two-dimensional Particle Image Velocimetry (PIV) measurements were taken at the mid-span of the wing, focussed on the upper surface, see Figure 1a. Hollow glass spheres of diameter 8 to 12 μm were used to seed the flow which were illuminated by a New Wave Solo Nd:YAG 50 mJ laser. Measurements were conducted with either a 4- or 8-megapixel CCD camera. All image pairs were processed with INSIGHT 4G using an interrogation window of 24 X 24 or 32 X 32 pixels, depending on the camera, with a grid overlap of 0.25 yielding resolutions 0.015*c* and 0.020*c* respectively. All transient PIV measurements are presented as the average of 100 phase-locked image pairs, whereas the impulsively started sinusoidal measurements are presented as the average of 30 phase-locked image pairs. The uncertainty of the averaged velocity measurements is estimated to be no greater than 2% of the freestream velocity [17]. This is based on the method of Charonko & Vlachos [18], where uncertainty is estimated with a 95% confidence level through the cross-correlation peak ratio between the primary and secondary correlation peaks. Vector uncertainties were calculated for each image pair using Insight 4G's validated algorithm [19]. The uncertainty of an averaged velocity vector is then calculated through,

$$\boldsymbol{\delta U_{avg}} = \frac{\boldsymbol{\delta U}}{\sqrt{\boldsymbol{N}}} \qquad \text{(Eq. 1)}$$

where δU_{avg} is the uncertainty of the averaged vector, δU is the uncertainty of a single vector and N is the number of PIV image pairs.

III. Results

Canonical Case

We first consider the aerodynamic response to a single transient plunging motion, denoted motion A, presented in Figure 2 (left column). As the airfoil plunges normal to the free stream with velocity *V*, an effective angle of attack is induced, denoted α_{pl}, where $\alpha_{pl} = tan^{-1}(V/U_\infty)$. The plunging motion considered is such that α_{pl} is increased linearly, held constant at a maximum, $\alpha_{pl,peak,A}$, for 0.05 c/U_∞, before decreasing linearly back to zero, as proposed by Ol

et al. [4]. Motion duration is held constant throughout at 2.22 convective times ($\tau = tU_\infty/c$). In addition, the non-dimensional plunge position (h/c) is plotted in blue to highlight the smooth transition into and out of plunging motion. The lift response relative to the static lift, ΔC_l, for α_0 = 5º (pre-stall) and 20º (post-stall) are presented on the second row (left column). This represents the change in lift from the static component as the airfoil is plunged at a fixed geometric angle of attack, α_0. The static lift coefficient for α_0 = 5º and 20º is C_l = 0.61 and 0.76 respectively. Likewise, ΔC_m represents the change in pitching moment from the static component. The static pitching moment coefficient for α_0 = 5º and 20º is C_m = -0.027 and -0.099 respectively. During plunging motion (within the grey band), ΔC_l displays a strikingly similar response for α_0 = 5º and 20º despite the differences in initial flow state, i.e. attached and fully separated flow respectively. The ΔC_l response during airfoil motion is a combination of added-mass and circulatory components. Assuming the theoretical estimate of Theodorsen [20] based on a projected chord length, the added-mass components of α_0 = 5º and 20º are largely similar and have been shown by Bull et al. [6] to account for approximately 30% of the peak lift during the same transient motion as Figure 2. In terms of the circulatory component, a transient motion of $\alpha_{pl,peak}$ = 25º and T = 2.22τ is reasonably aggressive and will rapidly take both α_0 = 5º and 20º far beyond the static stall angle (α_0 = 9 to 10º). For the same motion, Bull et al. [6] demonstrated the formation of a coherent LEV that dominates the flow field on both pre- and post-stall airfoils, which indicates the bulk of the circulation during motion is contained within the LEV [21]. The combination of a comparable added-mass, and an LEV dominated circulatory component may explain the similar responses in ΔC_l observed for α_0 = 5º and 20º (Figure 2).

In the post-motion stage, $\tau > 0$, significant differences can be observed. For α_0 = 5º, ΔC_l becomes negative before quickly approaching steady-state, whereas multiple large peaks of decaying magnitude are observed for α_0 = 20º. The post-motion peaks have been shown by Bull *et al.* [6] to be caused by the formation of additonal LEVs of decaying coherency, termed *large-scale vortex shedding*. These are shown in the insets of normalised spanwise vorticity for Figure 2. We denote these LEVs with the subscipt 1A, 2A and 3A, where the subscript inidicates the LEV cycle number and the motion that preceded (i.e. motion A). For the relative pitching moment, ΔC_m, large differences are observed during the motion, but mirror the behavior of ΔC_l in the post-motion phase. The reader is reffered to Bull *et al.* [6] for a full discussion of the aerodynamic responses to single transient moitions.

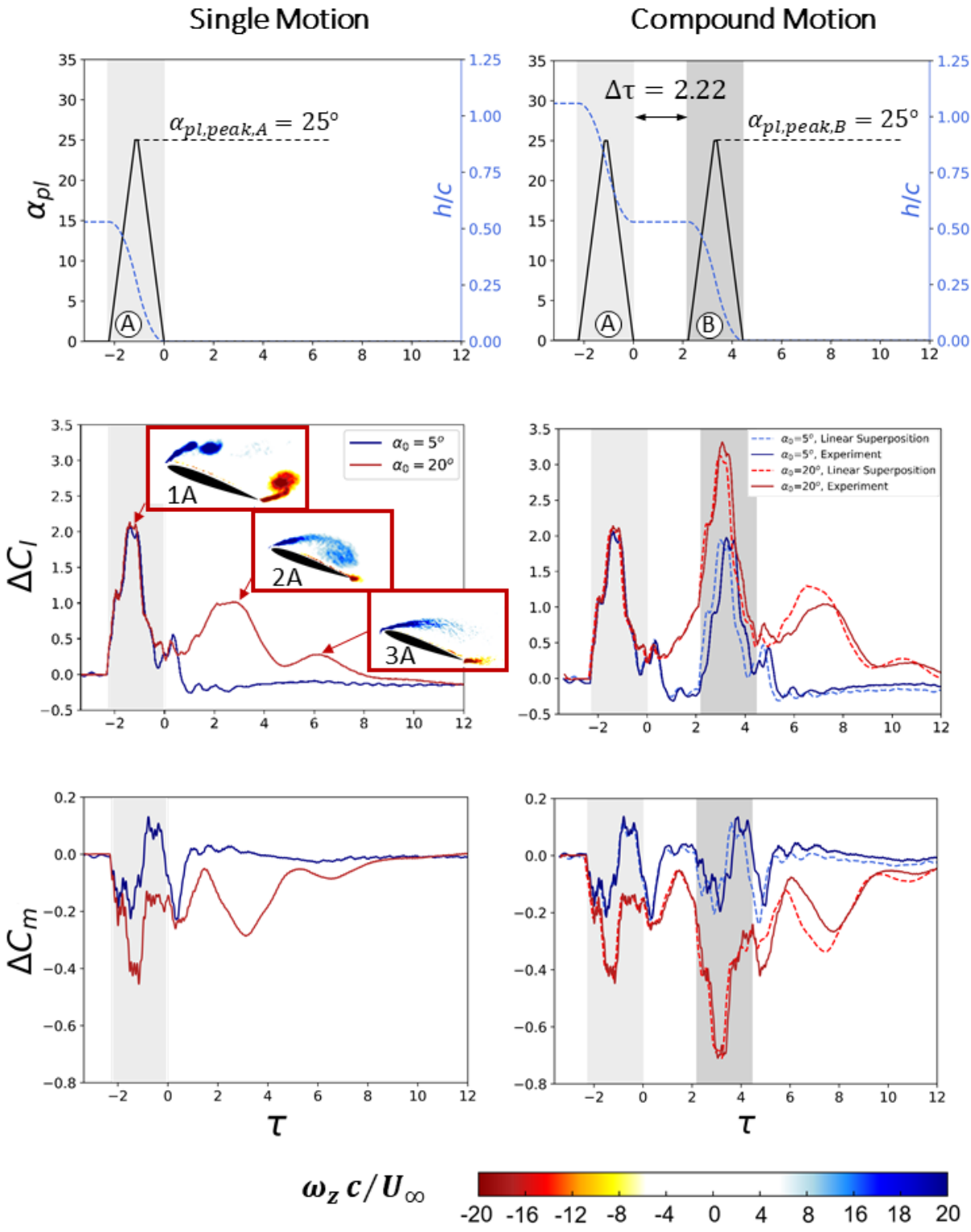

Figure 2: Profile of motion induced angle of attack, α_{pl}, and non-dimensional plunge position, *h*/c, with corresponding lift and pitching moment responses for single (left column) and compound transient (right column) motions.

Post-motion, large-scale vortex shedding is shown here to decay by τ = 12, but depending on conditions, this behavior can persist up to 15 convective times after the motion ends [6]. This decay rate shows strong dependence on geometric angle of attack, airfoil motion and airfoil geometry. A complete description is not included here for brevity and readers are referred to Bull *et al.* [6] for a full discussion. In Figure 2 (right column) a second motion, denoted motion B, is introduced within this window with a delay of $\Delta\tau$ = 2.22 (one motion period); that is motion B initiates 2.22 convective times after motion A has ended. Note that by defining the end of motion A as τ = 0, motion B inititates at $\tau = \Delta\tau$. In this case motion B is identical to motion A. Consider first the ΔC_l response for α_0 = 5º. Motion B begins where ΔC_l is negative at $\Delta C_l \approx -0.2$, and peak ΔC_l for motion B is observed to be smaller than for motion A. The opposite is true for α_0 = 20º. Here motion B initiates during a large-scale vortex shedding event, where $\Delta C_l \approx 1$, leading to a drastic increase in peak lift from ΔC_l = 2.1 to 3.3. From this it appears that the *change* in lift induced by motion B is similar to A, but the *total* lift depends on the state of the flow prior to motion B. With this in mind, the linear superpositon of the single motion responses (left colum) were constructed and plotted as dashed lines. These were created by time shifting the response of a single motion by $T+\Delta\tau$ and adding this to the original single motion response. For α_0 = 5º, the linear superposition prediction is in agreement with the experiment, albeit with a slight lead. For α_0 = 20º, the linear superposition prediction is in remarkable agreement with the experiment, particularly during motion, despite LEV formation prior to motion B. This slightly overpredicts the vortex shedding peak between $\tau \approx 6$ to 8 due to the additon of the third peak present in the single motion case (left column), before falling back into agreement as the shedding process decays. The pitching moment displays the same behavior as the lift and also exhibits good agreement between experiment and linear superposition, particularly during motion B.

Effect of Timing

Figure 2 demonstrates good performance of the linear superposition prediction regardless of the flow state prior to motion B. However, it is important not to overstate this result as it shows just one possible $\Delta\tau$ of motion B within the large-scale vortex shedding window. Figure 3 investigates the effect of different motion B timings from $\Delta\tau$ = 0.00 to 3.33 at α_0 = 20º with respect to ΔC_l and provides corresponding flow fields of normalised spanwise vorticitiy during the motion. For comparison purposes, the same phases during motion A for the single motion

case are presented on the top row. Only the lift responses are shown here and in general, the pitching moment was found to closely correspond to the lift in terms of linear superposition performance [17].

At $\Delta\tau = 0.00$ (Figure 3), the peak lift displays an increase during motion B, from $\Delta C_l \approx 2.1$ to 2.7. This is captured well by linear superposition, but soon falls out of agreement before motion end. From the flow field images, motion B initiates at $\tau = 0.00$ where LEV_{1A} is passing over the trailing-edge, just prior to initiating a TEV. As the motion progresses to $\alpha_{pl,peak}$, LEV_{1B} appears stronger and closer to the airfoil surface than for motion A (top row), which corresponds to the increase in peak lift during motion B. In addition, the TEV formed during motion B also appears stronger and more coherent than for motion A.

When $\Delta\tau = 1.11$, there is a further increase in peak lift during motion B, $\Delta C_l \approx 2.1$ to 3.3, and the subsequent shedding peaks are more pronounced. Linear superposition shows good agreement in this case, with only minor discrepencies in peak lift at $\tau \approx 6$. The corresponding flow field images show interesting behvaiour. When motion B initiates, the early stages of LEV_{2A} formation can be seen, along with a TEV triggered by the detachment of LEV_{1A}. During motion acceleration, $\tau = 1.67$ (second column), LEV_{2A} is cut-off from its feeding shear layer as the vorticity eminating from the leading-edge begins to roll-up into a new, more coherent vortex, i.e. LEV_{1B}. At $\tau = 2.22$, LEV_{2A} has been mostly consumed and its remnants can be seen stretching into LEV_{1B}. Interestingly at $\alpha_{pl,peak}$ there is an absence of a TEV. This could explain why the peak ΔC_l for $\Delta\tau = 1.11$ is larger than $\Delta\tau = 0.00$, due to the absence of a TEV and the associated downwash. This highlights the sensitivity of the response to the timing of motion B and where it situates within the large-scale vortex shedding cycle. For $\Delta\tau = 0.00$, the motion initates around the time where a TEV is about to form, whereas for $\Delta\tau = 1.11$ the timing of motion B occurs when the TEV has already been shed. By $\tau = 2.78$, LEV_{2A} and LEV_{1B} have fully combined into a single, larger structure.

The lift response for $\Delta\tau = 2.22$ has previously been discussed and so the focus here will be on the flow field behavior. The motion initiates at $\tau = 2.22$ where LEV_{2A} spans the entire upper surface. When the airfoil accelerates downwards, $\tau = 2.78$, LEV_{2A} is pinched-off due to the roll-up of the shear layer at the leading-edge (LEV_{1B}). At $\tau = 3.33$ the two vortical strucutres, LEV_{2A} and LEV_{1B}, display strong interaction. LEV_{1B} is lifted further from the airfoil surface as LEV_{2A}

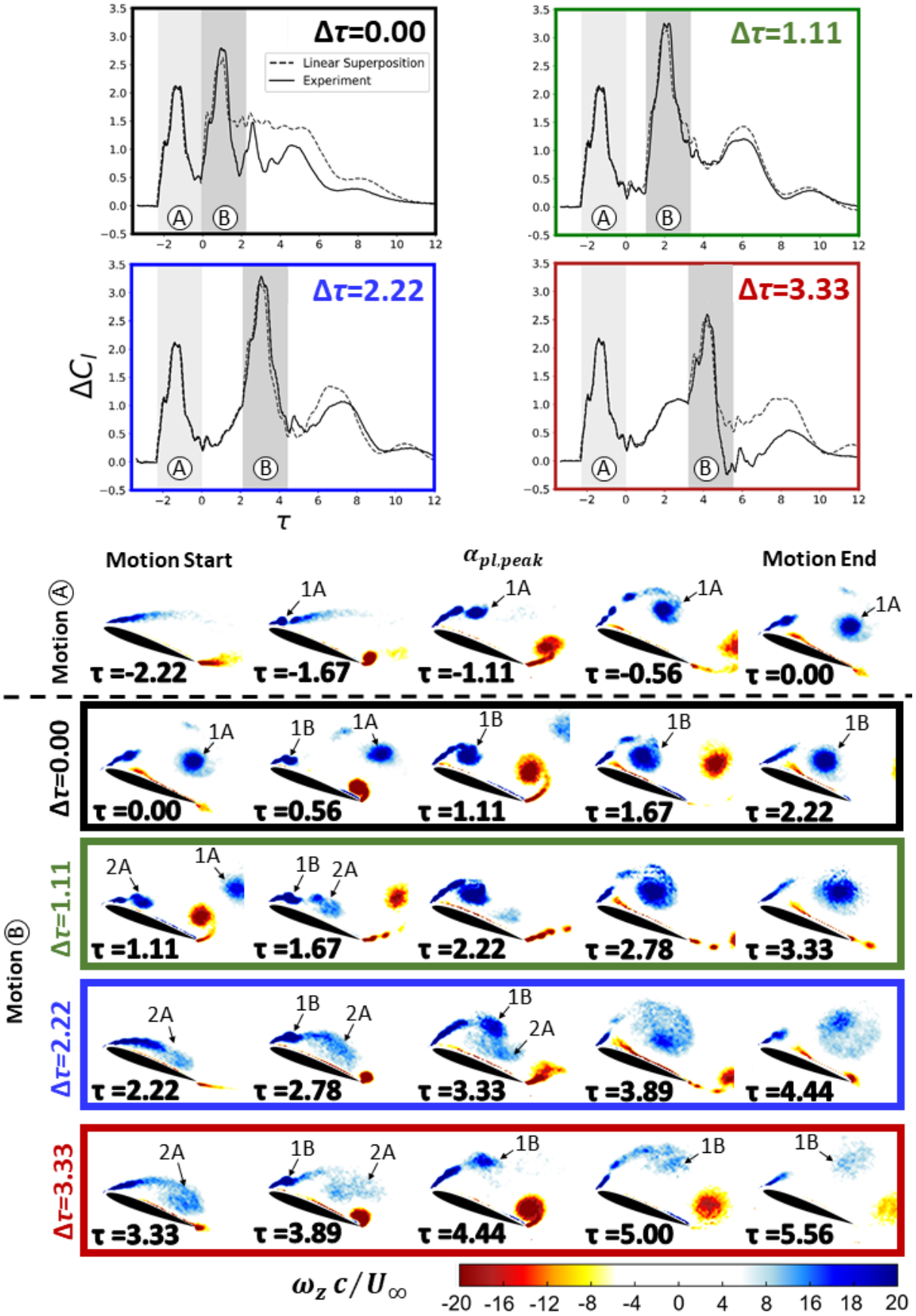

Figure 3: Lift responses for compound transient motion with varying motion delays, Δτ, and their comparison to the linear superposition prediction, alongside corresponding flow fields of normalised spanwise vorticity.

is stretched and forced underneath. Despite the inhomogenous structure of the combined LEVs, the peak lift remains high, perhaps again owing to the absence of a coherent TEV. The merged vortical structure then begins to rotate in a clockwise sense as it is convected downstream. A distinct spiral pattern is particularly apparent at τ = 4.44 that echoes the merging behavior of free, unequal strength, co-rotating vortex pairs documented by Trieling *et al.* [22].

The final case in Figure 3, $\Delta\tau$ = 3.33, illustrates where the timing of motion B is such that no vortex merging takes place and the linear superposition prediciton performs poorly. Motion B initiates at τ = 3.33, where LEV_{2A} is approaching the trailing-edge, just prior to TEV formation. As the airfoil accelerates, LEV_{2A} is pinched-off and LEV_{1B} begins to form. At this instant, a coherent TEV is observed forming in close proximity to the upper surface, which appears to distort LEV_{2A}. At $\alpha_{pl,peak}$, τ = 4.44, LEV_{2A} has been destroyed by the newly forming TEV, whilst LEV_{1B} is lifted further from the upper surface. Despite this, peak lift during motion B remains higher than motion A and linear superposition accurately captures the initial portion of motion B. The lift drops dramatically beyond τ > 4.44, even becoming negative around $\tau \approx$ 5. LEV_{1B} then displays a notable reduction in coherency as it convects downstream.

Figure 3 demonstrates that quasi-linear behavior of compound motions depends on the merging process of the LEVs on the upper surface, which itself is sensitive to the timing of motion B and where it falls in the cycle of large-scale vortex shedding. To explore this further, the correlation between the experimental and linear superposition signals were calculated across a range of $\Delta\tau$. This is presented in Figure 4, where a normalized correlation between the experimental and linear superposition signals is defined as,

$$\frac{\Delta C_{exp.} \cdot \Delta C_{lin.}}{\frac{1}{2}\left(\Delta C_{exp.} \cdot \Delta C_{exp.} + \Delta C_{lin.} \cdot \Delta C_{lin.}\right)} \qquad \text{(Eq. 2)}$$

where $\Delta C_{exp.}$ and $\Delta C_{lin.}$ are the relative lift or pitching moment signals for the experiment and linear superposition prediciton respectively. Equation 2 yields the dot product of the two signals divided by the average of the dot products of each signal with itself, resulting in a correlation value ranging from −1 to +1. The normalized correlation results presented in Figure 4 are calculated on a measurement window size of 10 convective times from the start of motion B. Figure 4 displays a distinct drop in correlation at $\Delta\tau$ = 3.33 for both the lift and

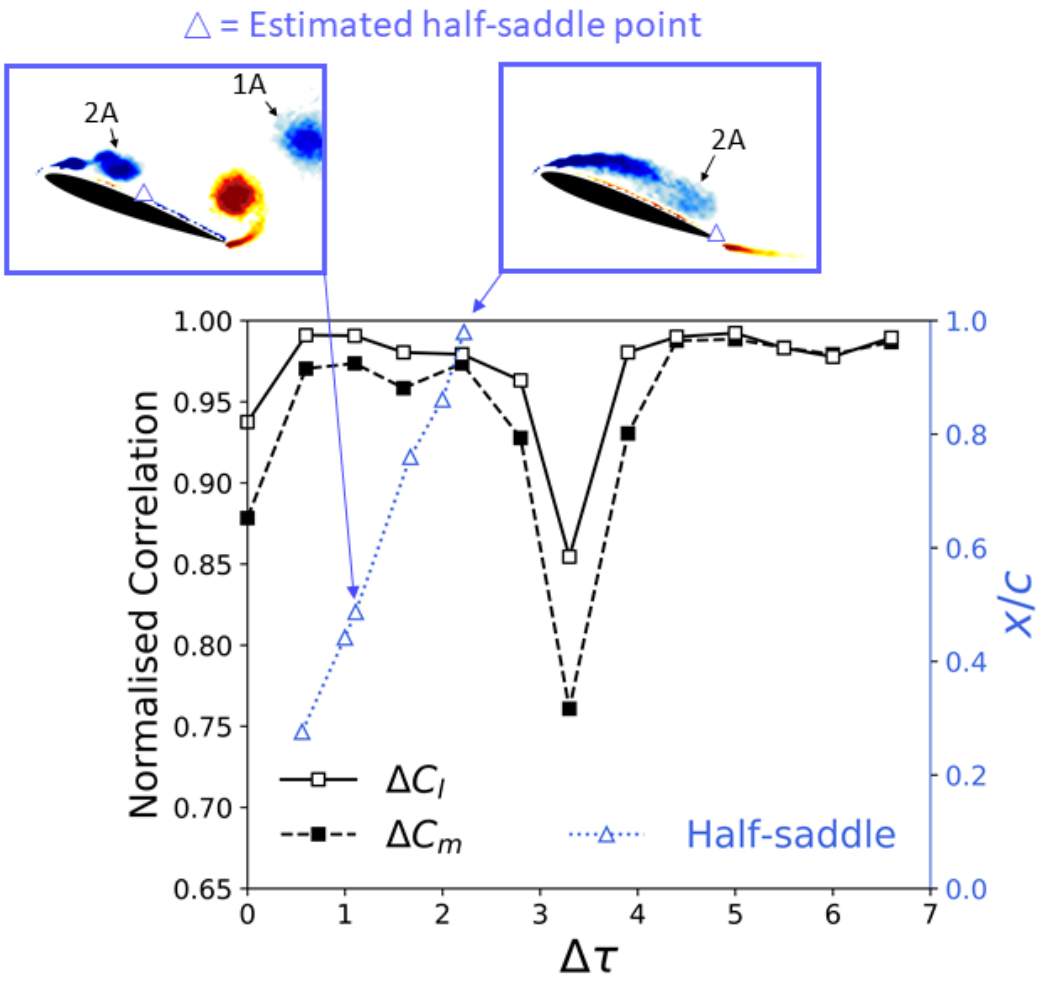

Figure 4: Axis 1 (black): Normalized correlation of lift and pitching moment responses with their linear superposition prediction for different motion delays, Δτ. Axis 2 (blue): Downstream half-saddle point for LEV_{2A}.

pitching moment signals, where TEV formation prevented constructive LEV merging (Figure 3). To corroborate this, the half-saddle point downstream of LEV_{2A} was extracted from the PIV measurements. This half-saddle point is defined where the bounding streamline around the LEV connects to the airfoil surface and was estimated from PIV data where the tangential velocity component at a distance of $0.02c$ above the airfoil surface transitioned from upstream (negative) to downstream (positive) flow. This is presented in Figure 4, where triangles on the PIV insets represent the estimated half-saddle point. The propagation of the half-saddle is superposed onto the plot of normalised correlation (shown in blue) and should be interpreted as the chordwise location of the half-saddle, downstream of LEV_{2A}, when motion B is initiated at $\tau = \Delta\tau$. When the half-saddle point is attached to the surface ($x/c < 1$), LEV_{2A} is still bound to the airfoil [23] and the correlation remains high when motion B is introduced due to

constructive merging of LEV_{2A} and LEV_{1B}. By $\Delta\tau$ = 2.22, the half-saddle has reached the trailing-edge (x/c = 0.98), beyond which the correlation drops. This marks the beginning of the LEV detachment process. The half-saddle leaves the trailing-edge to form a full-saddle point and TEV formation is initiated [24]. If motion B occurs in this short time window, $\tau \approx$ 2.5 to 4, a strong TEV is formed which disrupts constructive merging of LEV_{2A} and LEV_{1B}. Beyond $\Delta\tau$ = 3.33 the correlation quickly recovers and stays between 0.95 and 1.00, even in the presence of additonal weaker shedding cycles between τ = 6 and 7, see Figure 2.

Effect of Motion B Amplitude

The data presented in Figure 3 demonstrated reasonable performance of the linear superposition prediction where constructive LEV merging was observed. In these cases, LEV_{1B} appeared much stronger and exhibited dominant behavior over LEV_{2A}. Figure 5 explores the effect of strength ratio between LEV_{2A} and LEV_{1B} through a change in motion B amplitudes, $\alpha_{pl,peak,B}$ = 5, 10, 15, 20, 25º, at $\Delta\tau$ = 2.22. In order to construct the linear superposition of motion A and motion B with different amplitudes, single motion cases were conducted at $\alpha_{pl,peak}$ = 5, 10, 15, 20, 25º. These cases can then be used to construct the linear superposition signal for any combination of available amplitudes for motion A and motion B using the time shift method described earlier. Relative lift signals from both experiment and linear superposition prediction are presented alongside corresponding flow field images. Lift and flow field images for the single motion case are also presented for comparison. During motion B, linear superposition displays good agreement with the experiment for all $\alpha_{pl,peak,B}$, but consistently overpredicts the lift peak between τ = 6 and 8. As $\alpha_{pl,peak,B}$ is increased the lift peaks increase monotonically and there is a growing delay in the post-motion lift peak between τ = 6 and 8. The flow field images show increasing prominence of LEV_{1B} and its interaction with LEV_{2A} as $\alpha_{pl,peak,B}$ is increased, which tends to delay detachment of the merging vortical structure over the trailing-edge, see column τ = 4.44. This may explain the increasing delay of the lift peak between τ = 6 and 8.

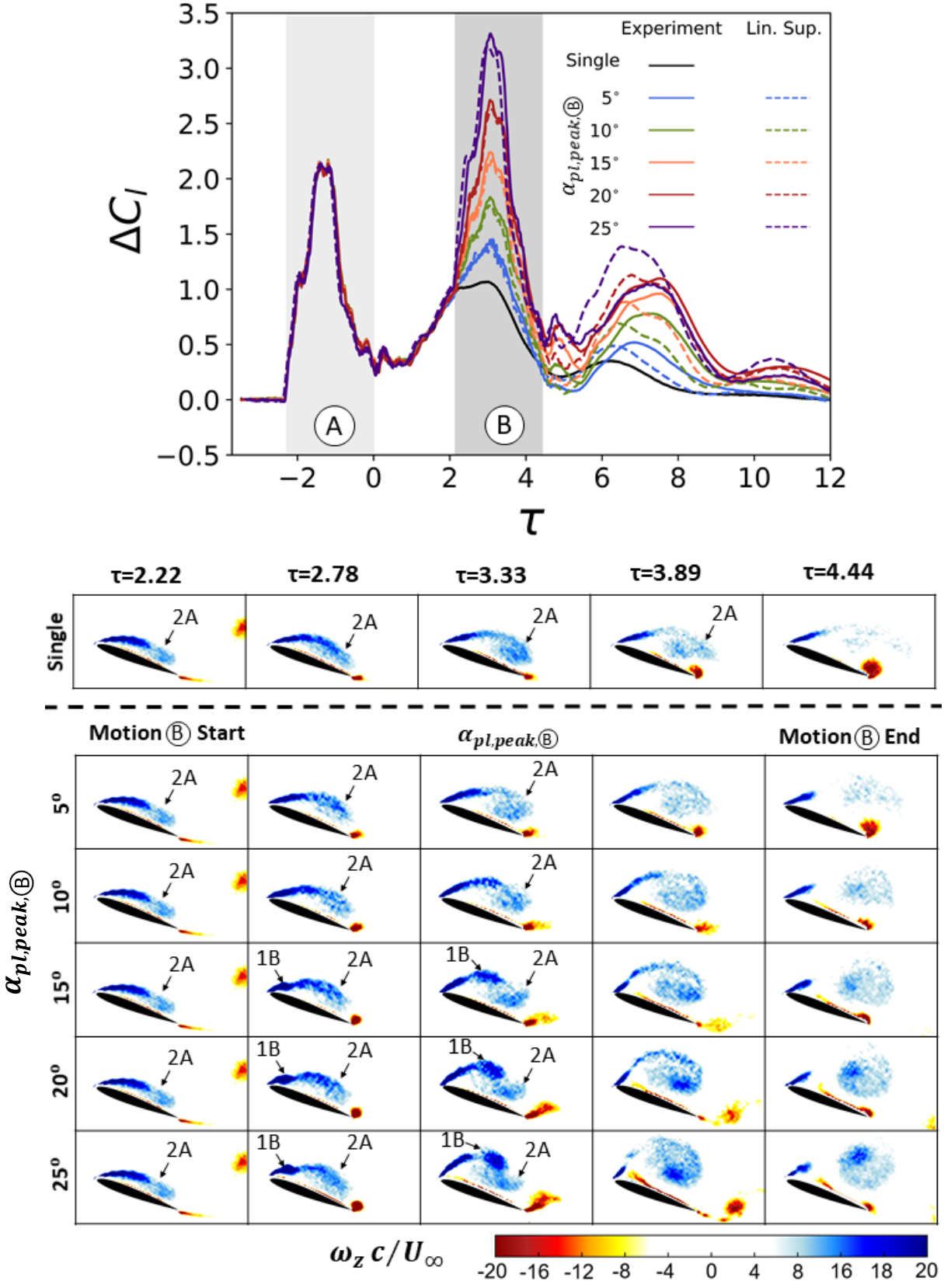

Figure 5: Relative lift responses with their linear superposition prediction for varying motion B amplitudes at Δτ=2.22, with corresponding flow fields of normalized spanwise vorticity.

Additional Transient Motions

Linear superposition has shown reasonably good agreement with experiment for two transient motions, particularly during the motion phase. In almost all cases however, this drifts out of agreement during post-motion shedding cycles (τ = 6 to 8, Figure 5) which will have a knock-on effect for the performance of linear superposition in the event of additional motions. Figure 6 explores the lift response to four identical transient motions with a constant delay between each motion from $\Delta\tau$ = 0.50 to 2.00. For these cases it was necessary to reduce the amplitude of the motion to $\alpha_{pl,peak}$ = 15° due to a total displacement constraint, i.e. tunnel wall proximity, but the motion period remains at T =2.22τ. All cases display an asymptotic rise in peak lift with each subsequent motion, which increases for higher values of $\Delta\tau$. At $\Delta\tau$ = 2.00, peak ΔC_l has almost doubled by the last transient motion. Interesingly the linear superposition prediction performs well, particularly for $\Delta\tau$ = 1.00. At $\Delta\tau$ = 2.00 a continuing drift from agreement can be seen from the first motion to the last, culminating in an underprediciton of the true lift response. This highlights the compounding effect of errors when using linear superpositon for certain values of $\Delta\tau$.

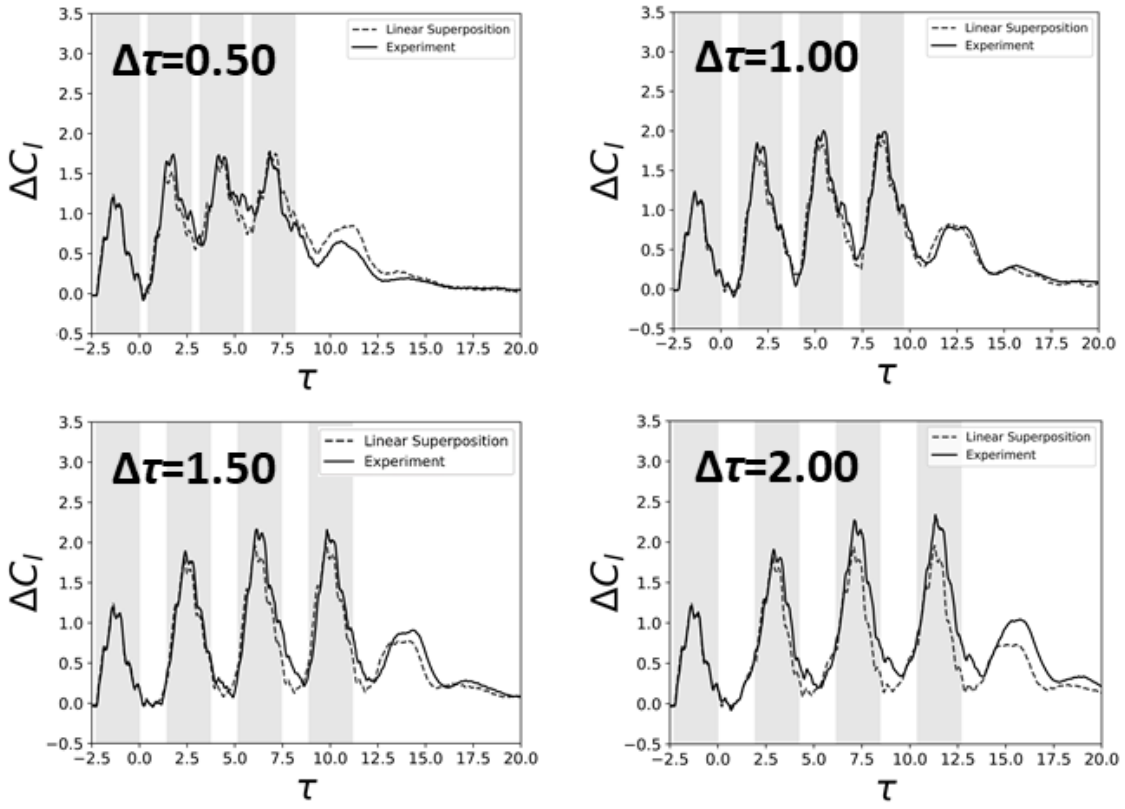

Figure 6: Compounding effects of four transient motions. Relative lift responses with their linear superposition prediction for varying motion delays.

Periodic Motion

Figure 6 points towards the establishment of periodic behavior, where the response no longer shows cycle-to-cycle variation in a phase-average sense. The lift maxima during each motion exhibit an asymptotic increase, which mirrors the mean lift increase for sinusoidally plunging airfoils [25, 26]. The aim of this section is to test the limits of the linear superposition principle until periodic conditions are achieved. All cases are performed at $\alpha_0 = 15^o$ to match the conditions of Chiereghin *et al.* [25]. Sinusoidal motions are defined through the reduced frequency, $k = \pi fc/U_\infty$, and plunging amplitude normalised by chord length, A/c, where A is the peak-to-peak amplitude.

Figure 7 presents the motion profiles and lift response for a single sinusoid (left column) and periodic sinusoidal motion (right column) at $k = 0.94$ and $A/c = 0.5$. Note that in these sinusoidal cases motion is initiated at $\tau = 0$. For the single sinusoid (left column), the lift response displays a single vortex shedding peak around $\tau \approx 7$ before decaying to approach steady-state by $\tau \approx 12$. For the periodic case (right column) the lift exhibits an asymptotic increase in mean lift, reaching periodic conditions in roughly 10 convective times. By summing the individual response, the periodic linear superposition response can be consructed. This is shown by the dashed line on the periodic case (right column). This asks the question; can the mean lift increase for periodic motion be described by the information contained within the vortex shedding of a single sinusoidal period?

Figure 8a presents the relative lift coefficient, ΔC_l, during impulsively started sinusoidal airfoil motion along with the linear superposition prediction. Corresponding flow fields of normalized spanwise vorticity at maximum α_{pl} for the first three motion periods are also presented in Figure 8b. A distinct increase in peak lift can be seen between the first and second period for $k = 0.24$ (Figure 8a). This is explained by the corresponding flow field images (Figure 8b) where a coherent LEV is present in periods 2 and 3. Linear superposition is able to capture the lift response with reasonable accuracy at this frequency, with the notable exception of the secondary peak present in the experiment. At $k = 0.47$ the difference between the first and second period becomes less distinct (Figure 8b). The amplitude displays reduced variation whilst the mean lift shows an increase with τ. This corresponds to an apparent strengthening of the LEV which moves closer to the airfoil between periods 1 and 2. Linear superposition provides a reasonable prediction but tends to slightly over-predict the mean lift. For $k = 0.63$ and 0.94, the flow field images not only indicate a strengthening of the LEV, but also a suppression of the TEV from period 1 to 2. The linear superposition response captures the lift

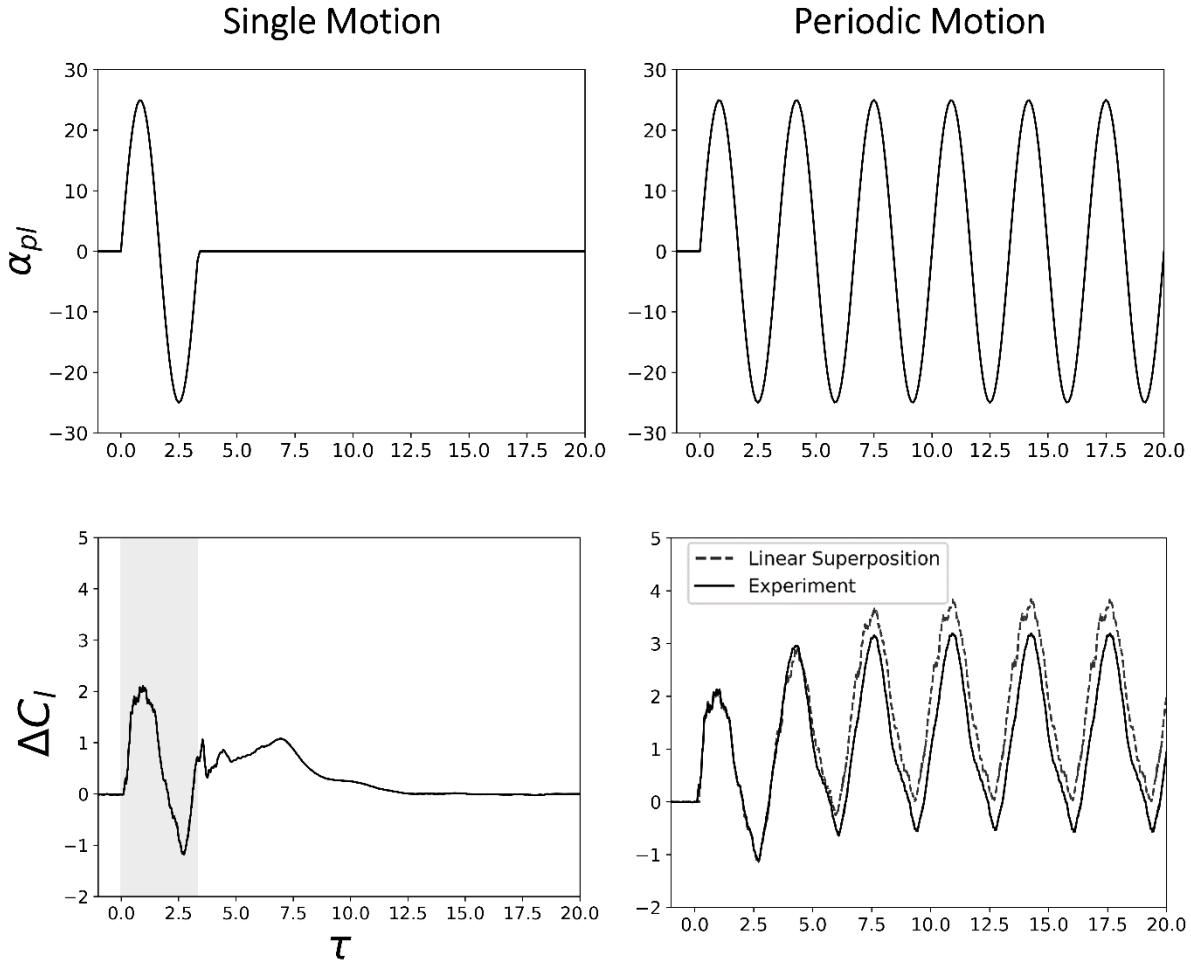

Figure 7: Profile of motion induced angle of attack, α_{pl}, and relative lift responses for single (left column) and periodic (right column), impulsively started sinusoidal motion.

maxima for $k = 0.63$, but significantly underpredicts the lift minima. Finally, at $k = 0.94$ the lift response amplitude is captured by linear superposition, due to the dominance of the added-mass component [25], whereas the mean lift component is drastically overpredicted.

To gain more insight into how the lift response develops, the mean and amplitude components of the lift signals were extracted. These are defined in Figure 9. The mean lift, $\overline{\Delta C_l}$, is tracked through a sliding average with a window of one motion period, giving a smooth variation with τ. Lift amplitude, $\Delta C_{l,a}$, was extracted through the difference between the period maxima and minima, giving a single point that was taken to occur mid-period.

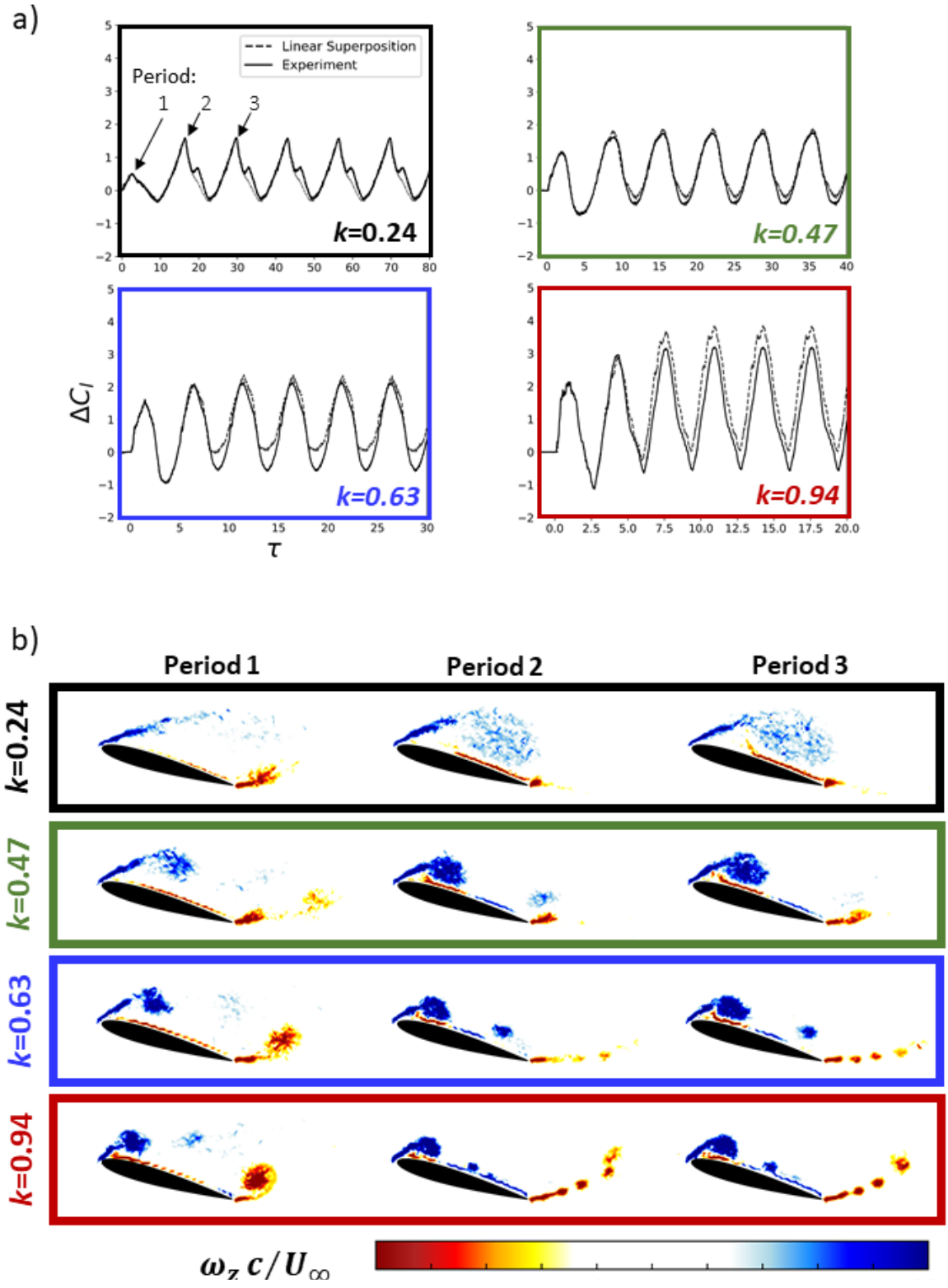

Figure 8: a) Relative lift responses for impulsively started sinusoidal motion with the linear superposition prediction for *k*=0.24, 0.47, 0.63 and 0.94; b) Corresponding flow fields of normalised spanwise vorticity at maximum α_{pl} for first three periods.

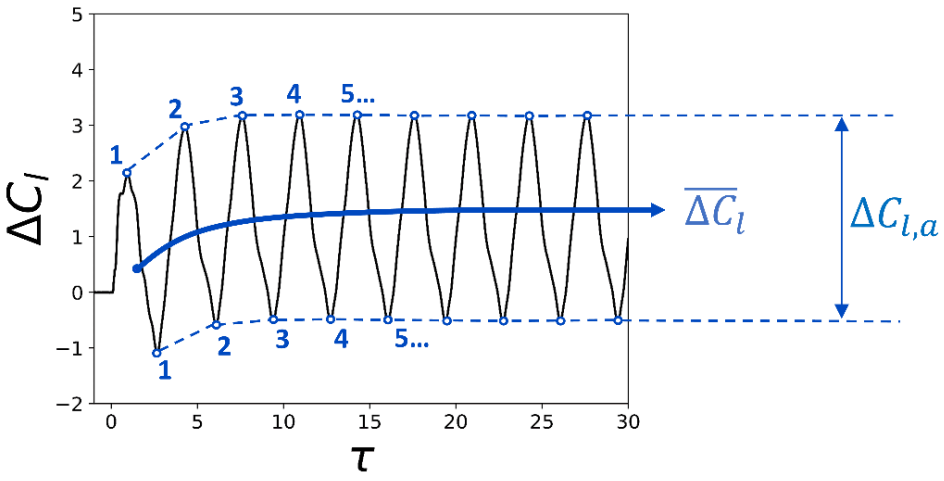

Figure 9: Methods of extracting mean relative lift, $\overline{\Delta C_l}$, and relative lift amplitude, $\Delta C_{l,a}$, against τ.

Figure 10 presents the results of this analysis for a range of reduced frequencies at a normalised plunging amplitude of A/c = 0.5. Note that the mean lift and lift amplitudes were normalised by their final periodic value, $\overline{\Delta C}_{l,\infty}$ and $\Delta C_{l,a,\infty}$ respectively, which were taken as the average of the last 30 periods from a 50-period run. All reduced frequencies display an asymptotic increase in mean lift to their final periodic value, see Figure 10a, which is reached within $\tau <$ 15. This increase can be attributed to the cyclic change in LEV formation, position, and coherency, as discussed earlier (Figure 8b), up to the establishment of the periodic wake. Multiple cycles are required to converge to periodic conditions for $0.47 \leq k \leq 0.94$ (see Figure 10b), whereas only one cycle is required for $0.16 \leq k \leq 0.24$. This reinforces the notion that the establishment of periodic conditions, in a phase-average sense, depends on convective time rather than the number of motion cycles, as the influence of the initial flow state is washed downstream [26]. Linear superposition manages to capture the asymptotic trend in mean lift but shows discrepancies in the normalised magnitude variation, particularly at higher frequencies. In terms of lift amplitude (Figure 10b) the lower frequencies display a greater variation from the first period; the higher frequencies on the other hand, $k \geq 0.63$, show little amplitude variation which again is most likely due to the added-mass effect as documented by Chiereghin *et al.* [25]. Linear superposition shows reasonable agreement with this trend, but differences in normalised magnitude variation start to appear at higher frequencies. Finally, Figures 10c and 10d present the mean lift and amplitude at periodic conditions for both the experiment and linear superposition prediction across a range of reduced frequencies and non-dimensional plunging amplitudes. The lift amplitude here is taken as the first harmonic of the signal calculated through the Fast Fourier Transform. Both mean lift and amplitude variations

are in line with the data presented by Chiereghin *et al.* [25]. For an amplitude to chord ratio A/c = 0.1, linear superposition shows good agreement in terms of the mean lift component for k < 0.47, Figure 10c. At higher frequencies, k > 0.47, the mean lift is progressively over-predicted. At A/c = 0.3 and 0.5, linear superposition slightly underpredicts the mean lift between k = 0.16 and 0.47, which most likely stems from the inability to capture the small secondary LEV peak present in the experiment lift signal, see Figure 8a. For k > 0.47 the mean lift is then

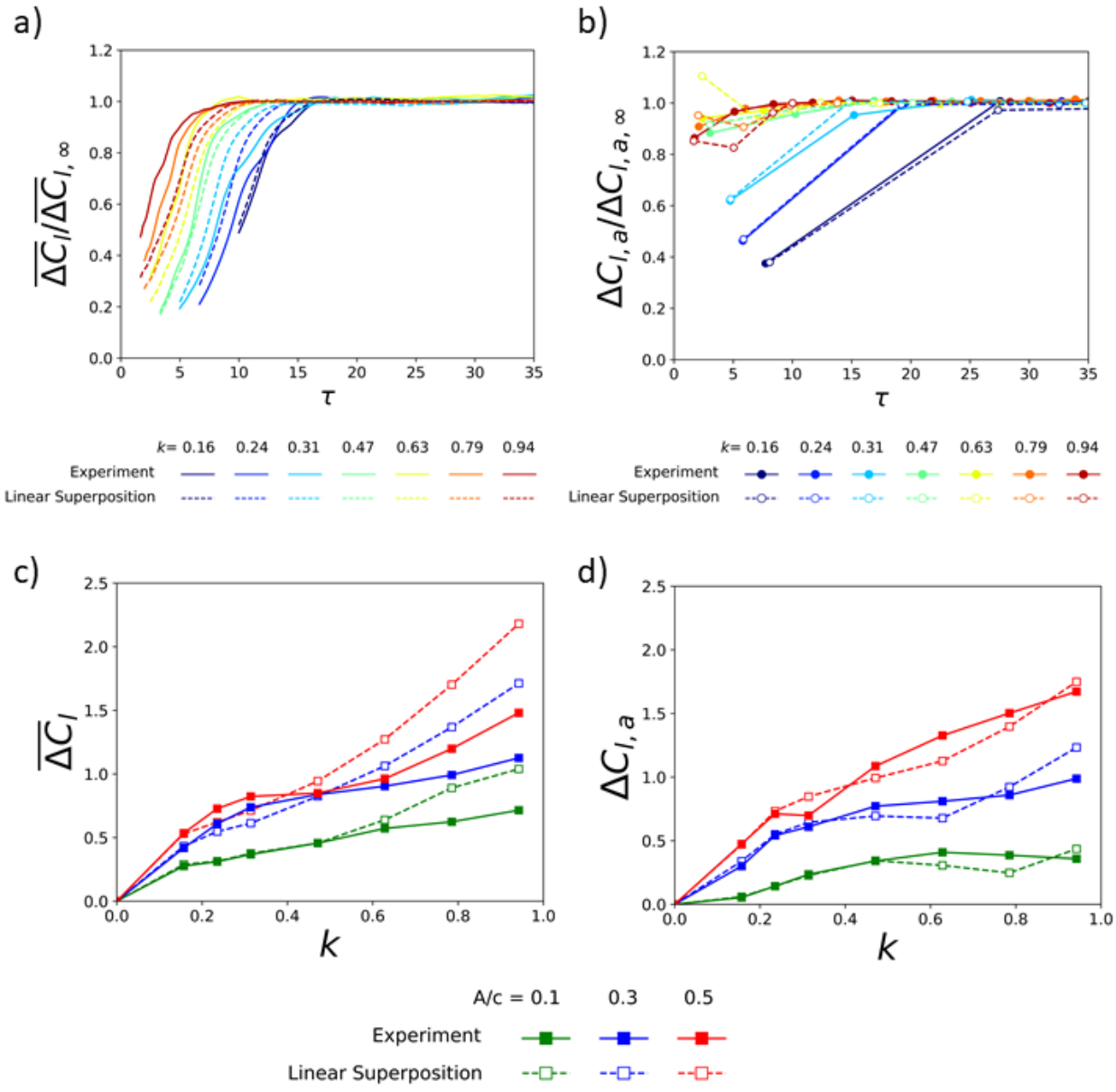

Figure 10: a) Normalized mean relative lift change for experiment and linear superposition signals, b) Normalized relative lift amplitude change for experiment and linear superposition signals. Comparison of periodic experiment and linear superposition signals for c) mean lift and, d) lift amplitude at driving frequency, obtained via Fast Fourier Transform.

significantly overpredicted by linear superposition. This is due to the continued summation of the single lift responses, which have been shown to take up 12 convective times to decay. At higher frequencies the mean lift predicted by linear superposition will begin to increase due to the accumulation of the lift in this decay period. In terms of lift amplitude, a reasonable level of agreement can be seen for all amplitudes, with the largest differences observed between k = 0.47 and 0.94. A better agreement in lift amplitude at high frequencies and amplitudes is expected however due to the dominance of the added-mass component.

Conclusions

The response to compounding transient motions has been investigated through lift, pitching moment and flow field measurements to investigate vortex behavior and to test the applicability of the linear superposition principle as a predictive tool in vortex dominated flows.

Significant increases in peak lift and nose-down pitching moment occurred at a post-stall angle of attack of 20º during the second of two transient motions. The lift and pitching moment responses could be reasonably estimated through linear superposition of the single motion responses with a surprising level of accuracy; quantified through a normalized correlation parameter. Flow field measurements revealed this performance to coincide with a constructive merging process of two LEVs on the upper surface. Breakdown of the linear superposition principle coincided with LEV detachment and the formation of a TEV that disrupted constructive LEV merging. The amplitude of the second motion showed minimal effect on LEV merging and subsequently the accuracy of the linear superposition prediction. It was found that linear superposition could accurately capture the lift response for up to four transient motions within certain conditions. Outside these conditions however, the prediction showed a significant drift from the true response, which could worsen for additional motions.

An extension to periodic motion was investigated, where linear superposition of a single, impulsively started sinusoidal cycle was compared with the true periodic response. This was found to capture the mean lift increase for $k < 0.47$, beyond which it displayed drastic over-prediction. Lift amplitude however was captured with reasonable accuracy across the range of reduced frequencies and amplitudes tested.

This study opens an interesting avenue for future research. Compound transient motions will need to be extended to different canonical unsteadiness, such as pitching, surging and gusts, to test for any commonality in vortex behavior. Although linear superposition performed well

with this specific plunging motion, it cannot be assumed that similar performance will be observed for other canonical motions.

Acknowledgements

The authors acknowledge the Engineering and Physical Sciences Research Council (EPSRC) Grant No. EP/M022307/1. The experimental studies made use of the Versatile Fluid Measurement System enabled through EPSRC strategic equipment grant funding (EP/M000559/1 and EP/K040391/1).

References

[1] Eldredge, J. D., and Jones, A. R., "Leading-Edge Vortices: Mechanics and Modeling," *Annual Review of Fluids*, Vol. 51, No. 1, 2019, pp. 75-104.
doi: 10.1146/annurev-fluid-010518-040334

[2] Manar, F., Mancini, P., Mayo, D., and Jones, A. R., "Comparison of Rotating and Translating Wings: Force Production and Vortex Characteristics," *AIAA Journal*, Vol. 54, No. 2, 2016, pp. 519-530.
doi: 10.2514/1.J054422

[3] Leknys, R. R., Arjomandi, M., Kelso, R. M., and Birzer, C. H., "Leading-edge vortex development on a pitching flat plate with multiple leading-edge geometries," *Experimental Thermal and Fluid Science*, Vol. 96, 2018, pp. 406-418.
doi: 10.1016/j.expthermflusci.2018.03.001

[4] Ol, M. V., Eldredge, J. D., and Wang, C., "High-Amplitude Pitch of a Flat Plate: An Abstraction of Perching and Flapping," *International Journal of Micro Air Vehicles*, Vol. 1, No. 3, 2009, pp. 203-216.
doi: 10.1260/175682909789996186

[5] Perrotta,G., and Jones, A. R., "Quasi-Steady Approximation of Forces on Flat Plate due to Large-Amplitude Plunging Maneuvers," *AIAA Journal*, Vol. 56, No. 11, 2018, pp. 4232-4242.
doi: 10.2514/1.J057194

[6] Bull, S. C., Chiereghin, N., Gursul, I., and Cleaver, D. J., "Unsteady Aerodynamics of a Plunging Airfoil in Transient Motion," *Journal of Fluids and Structures*, Vol. 103, 2021, pp. 103288.
doi: 10.1016/j.jfluidstructs.2021.103288

[7] Mulleners, K., Mancini, P., and Jones, A. R., "Flow Development on a Flat-Plate Wing Subjected to a Streamwise Acceleration," *AIAA Journal*, Vol. 55, No. 6, 2017, pp. 2118-2122.
doi: 10.2514/1.J055497

[8] Manar, F., and Jones, A. R., "An Evaluation of Potential Flow Models for Unsteady Separated Flow with Respect to Experimental Data," *Physical Review Fluids*, Vol. 4, No. 3, 2019, pp. 034702.
doi: 10.1103/PhysRevFluids.4.034702

[9] Perrotta, G., and Jones, A. R., "Unsteady forcing on a flat-plate wing in large transverse gusts," *Experiments in Fluids*, Vol. 58, No. 3, 2017, pp. 1-11.
doi: 10.1007/s00348-017-2385-z

[10] Corkery, S., Babinsky, H., and Harvey, J. K, "On the development and early observations from a towing tank-based transverse wing-gust encounter test rig," *Experiments in Fluids*, Vol. 59, No. 135, 2018, pp. 1-16.
doi: 10.1007/s00348-018-2586-0

[11] Biler, H., Badrya, C., and Jones, A. R., "Experimental and Computational Investigation of Transverse Gust Encounters," *AIAA Journal*, Vol. 57, No. 11, 2019, pp. 4608-4622.
doi: 10.2514/1.J057646

[12] Qian, Y., Wang, Z., and Gursul, I., "Interaction of Quasi-Two-Dimensional Vortical Gusts with Swept and Unswept Wings," *AIAA Scitech 2021 Forum*, Virtual Event, 2021, pp. 1-22.

[13] McGowan, G. Z., Granlund, K., Ol, M. V., Gopalarathnam, A., and Edwards, J. R., "Investigations of Lift-Based Pitch-Plunge Equivalence for Airfoils at Low Reynolds Numbers," *AIAA Journal*, Vol. 49, No. 7, 2011, pp. 1511-1524.
doi: 10.2514/1.J050924

[14] Elfering, K.H., and Granlund, K. O., "Lift Equivalence and Cancellation for Airfoil Suge-Pitch-Plunge Oscillations," *AIAA Journal*, Vol. 58, No. 11, 2020, pp. 4629-4643.
doi: 10.2514/ 1.J059068

[15] Xu, X., and Lagor, F. D., "Quasi-steady effective angle of attack and its use in lift-equivalent motion design," *AIAA Journal*, Vol 59, No. 7, 2021, pp. 2613-2626.
doi: 10.2514/1.J059663

[16] Heathcote, S. F., "Flexible Flapping Airfoil Propulsion at Low Reynolds Numbers," Ph.D. Dissertation, Department of Mechanical Engineering, The University of Bath, Bath, UK, 2006.

[17] Bull, S. C., "Unsteady Aerodynamics of Wings in Extreme Conditions," Ph.D. Dissertation, Department of Mechanical Engineering, The University of Bath, Bath, UK, 2020.

[18] Charonko, J. J., and Vlachos, P. P., "Estimation of uncertainty bounds for individual particle image velocimetry measurements from cross-correlation peak ratio," *Measurement Science and Technology*, Vol. 24, No. 6, 2013, 065301.
doi: 10.1088/0957-0233/24/6/065301

[19] TSI., "Uncertainty Analysis for PIV Measurement. ITTC Recommended Procedures and Guidelines," 017:2013–2014, 2008.

[20] Theodorsen, T., "General Theory of Aerodynamic Instability and the Mechanism of Flutter," NACA Technical Report NACA-TR-496, 1935, pp. 413–433.

doi: 10.1016/S0016-0032(35)92022-1

[21] Pitt Ford C. W., Babinsky H., "Impulsively started flat plate circulation," *AIAA Journal*, Vol. 52, No. 8, 2014, pp. 1800–1802.

https://doi.org/10.2514/1.J052959

[22] Trieling, R., R., Velasco Fuentes, O. U., and van Heijst, G. J. F., "Interaction of two unequal corotating vortices," *Physics of Fluids*, Vol. 17, No. 8, 2005, pp. 1-17.

doi: 10.1063/1.1993887

[23] Krishna, S., Green, M. A., and Mulleners, K., "Flowfield and Force Evolution for a Symmetric Hovering Flat-Plate Wing," *AIAA Journal*, Vol. 56, No. 4, 2018, pp. 1360-1371.

doi: 10.2514/1.J056468

[24] Widmann, A., and Tropea, C., "Reynolds number influence on the formation of vortical structures on a pitching flat plate," *Interface Focus*, Vol. 57, 2017, 20160079.

doi: 10.1098/rsfs.2016.0079

[25] Chiereghin, N., Cleaver, D. J., and Gursul, I., "Unsteady Lift and Moment of a Periodically Plunging Airfoil.," *AIAA Journal*, Vol. 57, No. 1, 2019, pp. 208-222.

doi: 10.2514/1.J057634

[26] Bull, S. C., Chiereghin, N., Cleaver, D. J., and Gursul, I., "Novel Approach to Leading-Edge Vortex Suppression," *AIAA Journal*, Vol. 58, No. 10, 2020, pp. 4212-4227.

doi: 10.2514/1.J059444